International Urogynecology Journal (2023) 34:3023–3032
https://doi.org/10.1007/s00192-023-05645-8

ORIGINAL ARTICLE

Somatic and autonomic nerve density of the urethra, periurethral tissue, and anterior vaginal wall: an immunohistochemical study in adult female cadavers

Erryn E. Tappy[1] · Denise M. O. Ramirez[2] · Abby M. Stork[1] · Kelley S. Carrick[3] · Jennifer J. Hamner[4] · Jessica E. Pruszynski[1] · Marlene M. Corton[1]

Received: 16 June 2023 / Accepted: 18 August 2023 / Published online: 5 October 2023

Abstract

Introduction and hypothesis Retropubic procedures may disrupt nerves supplying the pelvic viscera; however, knowledge of pelvic neuroanatomy is limited. We sought to characterize somatic and autonomic nerve density within the urethra, periurethral tissue, and anterior vagina.

Methods Axial sections were obtained from pelvic tissue harvested from female cadavers ≤24 h from death at three anatomical levels: the midurethra, proximal urethra, and upper trigone. Periurethral/perivesical tissue was divided into medial and lateral sections, and the anterior vagina into middle, medial, and lateral sections. Double immunofluorescent staining for beta III tubulin (βIIIT), a global axonal marker, and myelin basic protein (MBP), a myelinated nerve marker, was performed. Threshold-based automatic image segmentation distinguished stained areas. Autonomic and somatic density were calculated as percentage of tissue stained with βIIIT alone, and with βIIIT and MBP respectively. Statistical comparisons were made using nonparametric Friedman tests.

Results Six cadavers, aged 22–73, were examined. Overall, autonomic nerve density was highest at the midurethral level in the lateral and middle anterior vagina. Somatic density was highest in the external urethral sphincter (midurethra mean 0.15%, SD ±0.11; proximal urethra 0.19%, SD ±0.19). Comparison of annotated sections revealed significant differences in autonomic density among the lateral, medial, and middle vagina at the midurethra level (0.71%, SD ±0.48 vs 0.60%, SD ±0.48 vs 0.70%, SD ±0.63, p=0.03). Autonomic density was greater than somatic density in all sections.

Conclusions Autonomic and somatic nerves are diffusely distributed throughout the periurethral tissue and anterior vagina, with few significant differences in nerve density among sections analyzed. Minimizing tissue disruption near urethral skeletal muscle critical for urinary continence may prevent adverse postoperative urinary symptoms.

Keywords Neuroanatomy · Nerve density · Anterior vaginal wall · Retropubic space · Urinary incontinence

Introduction

The anterior vaginal wall and periurethral tissue are common sites for dissection during urogynecological procedures. Midurethral slings are placed at the level of the midurethra, between the anterior vaginal wall and urethra following dissection of this plane from a vaginal approach. The periurethral tissue is perforated to differing degrees to enter the retropubic space during retropubic and pubovaginal sling placement. Periurethral tissue is also disrupted during suture placement in retropubic colposuspension procedures. Anterior colporrhaphy requires dissection of the anterior vaginal wall and suture placement through fibromuscular tissue of the vagina.

✉ Marlene M. Corton
marlene.corton@utsouthwestern.edu

[1] Department of Obstetrics and Gynecology, UT Southwestern Medical Center, 5323 Harry Hines Blvd G6.238, Dallas, TX 75390, USA

[2] Department of Neurology and Neurotherapeutics, UT Southwestern Medical Center, Dallas, TX, USA

[3] Department of Pathology, UT Southwestern Medical Center, Dallas, TX, USA

[4] Department of Urogynecology, Indiana University Health, Carmel, IN, USA

The aforementioned procedures may disrupt the nerve supply to the anterior vaginal wall and periurethral tissue, which may contribute to post-operative voiding or sexual dysfunction [1, 2]. A meta-analysis of sexual function following midurethral sling placement found 33% of women experienced worsening sexual function postoperatively [3]. Rates of de novo sexual dysfunction after Burch colposuspension as high as 63.4% have been reported [4]. De novo voiding and sexual dysfunction have been reported after sacrocolpopexy, even in absence of anti-incontinence procedures [5–7]. On the other hand, these procedures are also associated with significant improvements sexual function, resolution of incontinence and prolapse related symptoms and overall improvement in patients' quality of life [7–9]. Given this, it is important to better understand precise areas of high nerve density within the periurethral tissue and anterior vaginal wall to avoid adverse outcomes potentially associated with disruption of nerves supplying this tissue.

To date, detailed understanding of nerve density within the periurethral tissue and anterior vaginal wall remains limited. Although gross dissections have mapped major nerves and plexuses of the pelvis and perineum, such studies fail to quantify and distinguish between autonomic and somatic nerves [10–14]. A number of histological studies have examined innervation of the urethra and neurovascular anatomy of the anterior vaginal wall [15–18]. However, studies describing the density of nerve subtypes in the periurethral tissue and anterior vaginal wall are lacking. Thus, the objective of this study was to characterize the density of autonomic and somatic nerve fibers within the urethra, periurethral tissue, and anterior vaginal wall.

Materials and methods

Following Institutional Review Board exemption, in accordance with the Code of Federal Regulations, Title 45, cadavers obtained from the Willed Body Program at the University of Texas Southwestern Medical Center (UTSW) in Dallas were examined. En bloc pelvic sections were harvested from adult female cadavers within 24 h of death utilizing methods similar to those from previously published work [19]. Cadavers with a history of gynecological cancer, gross anatomical alterations, or evidence of prior pelvic or vulvar surgery were excluded. Demographic data including age, race, body mass index, cause of death, and mode of delivery, if applicable, were collected when available. Preparatory dissections were performed by the senior author (M.M.C) with two other authors (E.E.T and J.J.H) to standardize a technique of tissue harvesting.

Gross dissection

En bloc pelvic sections were collected and fixed in 10% formalin solution for a minimum of 48 h then cut into 5-mm cross-sections perpendicular to the long axis of the urethra to the lateral boundary of the arcus tendineus fascia pelvis (ATFP) at three distinct levels denoted as the midurethra, proximal urethra, and upper trigone. Midurethral sections were cut starting 1 cm distal to the urethrovesical junction and extended just proximal to the pubic symphysis; proximal urethra sections extended from the bladder neck to 1 cm distal to the urethrovesical junction; upper trigone sections included the ureteric orifices (Fig. 1). Each anatomical level correlates with relevant anatomy encountered during retropubic and vaginal procedures. The midurethra is relevant to the placement of retropubic slings where trocars and mesh are passed and positioned, and placement of the distal Burch colposuspension sutures. The proximal urethra approximates the urethrovesical junction, a landmark used for the placement of proximal colposuspension sutures and pubovaginal slings. The upper trigone region increases the complexity of bladder injury and repair, and is included in the plane of dissection for anterior colporrhaphy.

Microscopic examination

Tissue sections were submitted in standard Surgipath IP II cassettes (measuring 1.12 × 1.61 × 0.26 in or 2.84 × 4.09 × 0.66 cm) or Super Mega cassettes (measuring 3 × 2 × 0.75 in or 7.62 × 5.08 × 1.90 cm; Leica Microsystems, Buffalo Grove, IL, USA) for tissue processing. Tissue was embedded in paraffin, sectioned and stained with hematoxylin and eosin (H&E) using standard methods by the UTSW Histo Pathology Core. Histological analysis was performed by a gynecological pathologist (K.S.C) and authors (M.M.C., E.E.T, J.J.H, and A.S) using a Nikon Eclipse 80i microscope (Nikon Inc, Los Angeles, CA, USA). At each anatomical level, histological examination was performed to outline and assess the composition of the urethra, periurethral/perivesical tissue, and anterior vaginal wall. The inner smooth muscle and outer skeletal muscle layers of the urethra were outlined and analyzed separately. The periurethral/perivesical tissue was outlined from the lateral aspect of the smooth muscle of the urethral wall to the medial aspect of the levator ani muscle; the medial aspect of the levator muscle was used as a surrogate for the ATFP, as this latter structure could not be accurately distinguished from the periurethral/perivesical connective tissue. Centered on clinical significance, the periurethral/perivesical tissue was further outlined by dividing the total width in half, resulting in a medial section in proximity to the urethra and a lateral section in proximity to the pelvic sidewall. The anterior vaginal wall was outlined and extended to a lateral boundary marked by the anterior sulci. The vagina was further outlined into middle, medial, and lateral sections. The middle section was bounded bilaterally by the lateral aspects of the smooth muscle of the urethral wall and represents the portion of the vagina in direct contact with the urethra. The

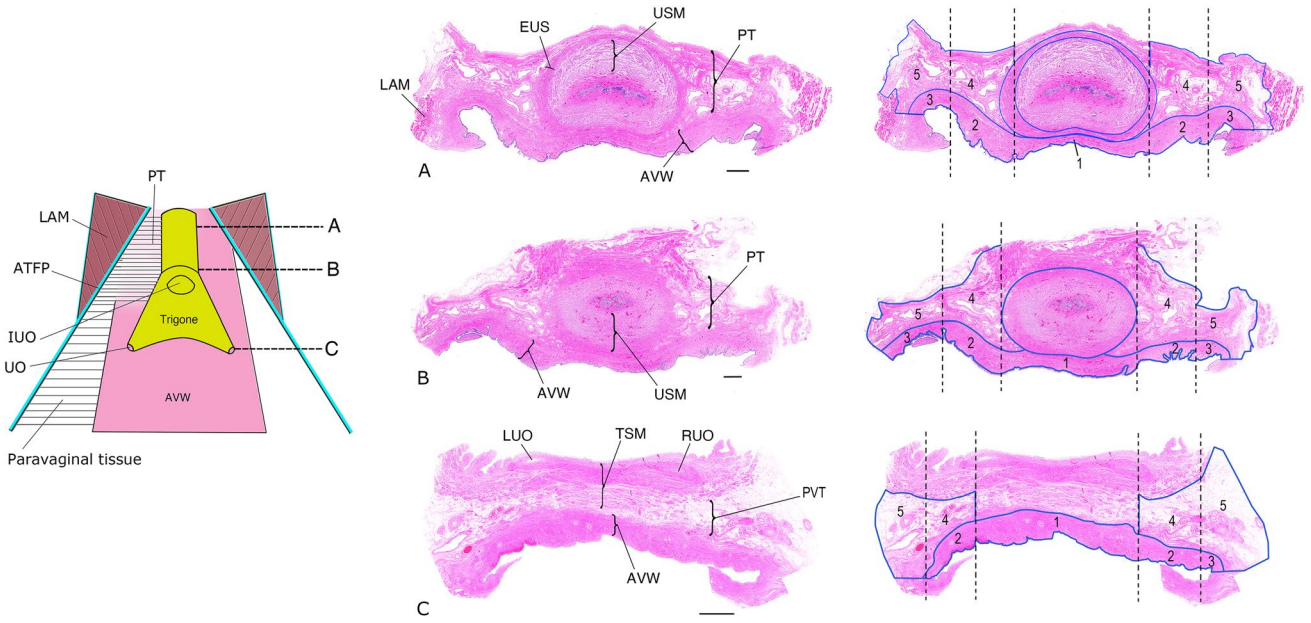

Fig. 1 Anatomical levels and histological sections were analyzed. Left panel is a schematic representation of the levels examined: **A** midurethra; **B** urethrovaginal junction; **C** upper trigone. Middle panel displays hematoxylin and eosin (H&E) staining corresponding to levels **A**, **B**, and **C**. Right panel is representative H&E with outlined regions individually analyzed for somatic and autonomic nerve density: *1*, middle anterior vagina; *2*, medial anterior vagina; *3*, lateral anterior vagina; *4*, medial periurethral tissue; *5*, lateral periurethral tissue. Key anatomical structures are labeled. *ATFP* arcus tendineus fascia pelvis, *AVW* anterior vaginal wall, *EUS* external urethral sphincter, *IUO* internal urethral opening, *LAM* levator ani muscle, *LUO* lower ureteric orifice, *PT* periurethral tissue, *PVT* perivesical tissue, *RUO* right ureteric orifice, *TSM* trigone smooth muscle, *UO* ureteric orifice, *USM* urethral smooth muscle. Scale bars for **A** and **B** are 2 mm and for **C** 5 mm

remaining total width of the vaginal wall lateral to the smooth muscle of the urethra was divided in half to create medial and lateral sections in proximity to the urethra and pelvic sidewall respectively (Fig. 1).

Immunostaining

Slides were deparaffinized, rehydrated, and subjected to antigen retrieval in sodium citrate buffer using a pressure cooker. After permeabilization with 0.2% (v/v) Triton X-100 in phosphate buffered saline and blocking in normal goat serum (NGS), primary antibodies were incubated overnight at 4°C and diluted in PBS containing 5% (v/v) NGS and 0.2% (v/v) Triton X-100. A rabbit polyclonal antibody directed against beta III tubulin (βIIIT; Abcam #ab18207; 1:200), a global axonal marker, and a mouse monoclonal antibody directed against Myelin Basic Protein (MBP; EMD Millipore # NE-1019; 1:200), a myelinated nerve marker, were used. After washing, secondary antibodies (goat anti-rabbit AlexaFluor 568, Invitrogen #A11036 and goat anti-mouse AlexaFluor 647, Invitrogen #A21236) were diluted 1:500 in PBS+5% NGS+0.2% Triton and incubated for 2 h. Slides were washed, and DAPI was stained and coverslipped with Fluoromount-G (SouthernBiotech #0100-01).

Slide scanning and annotation

Whole-slide, multichannel images of the immunostained slides were acquired at 10× magnification on the Zeiss Axioscan.Z1 in the Whole Brain Microscopy Facility at UT Southwestern (RRID:SCR_017949). All four fluorescent channels were acquired (blue, green, red, and far red) to allow use of the green channel autofluorescence as a reference for tissue structural details. All images were acquired using the same settings. Images were transferred to the UTSW high-performance computing cluster (BioHPC) for annotation, segmentation, and analysis. Annotations of individual anatomical sections of interest were manually drawn in Zeiss Zen Blue following review of adjacent H&E-stained slides.

βIIIT and MBP segmentation

Raw fluorescence images were brightness and contrast adjusted to the same settings for all images. Positive βIIIT and MBP staining were segmented using a manually determined threshold value based on visual distinction between positive and background areas. Double-positive βIIIT and MBP staining were segmented by taking the overlap between individual βIIIT and MBP segmentation maps. The percentage positive area within

each annotated section was calculated by taking the number of segmented pixels in each map divided by the total number of pixels in the annotation section (e.g., nerve density). Areas stained only with βIIIT antibodies (corresponding to unmyelinated nerves) were used as the measurement of autonomic nerve density, and the sum of areas double-positive for βIIIT and MBP together with areas that were only MBP positive (corresponding to myelinated nerves) were used as the measurement of somatic nerve density. Total nerve density was calculated as the sum of all positive pixel areas (βIIIT alone, MBP alone, and double positive) divided by the total area.

Statistical analysis

Within each anatomical level, annotated sections of the urethra, periurethral/perivesical tissue, and anterior vaginal wall were compared to detect differences in total, autonomic, and somatic nerve density. Statistical comparisons were made between individual sections of interest at each anatomical level using the nonparametric Friedman test owing to the dependent (comparisons made within cadavers) and skewed nature of the data. A p value of <0.05 was considered significant. All statistical analyses were performed using R version 3.6.1 (R Core Team, Vienna, Austria).

Results

A total of 6 adult female cadavers were examined with a median age of 28.5 years (range 22–73 years). Five cadavers were nulliparous aged 22–47 years old. Four cadavers were white, 1 Black, and 1 Hispanic. The median body mass index was 22.8 kg/m^2 (range 11.5–68.3 kg/m^2). The most common cause of death was complications of respiratory disease. Owing to size limitations of histological tissue processing and in some cases tissue degradation during immunostaining, representative slides for all cadaveric specimens were not available for all levels (Table 1).

Histological findings

In all specimens, the smooth muscle of the inner urethral wall was encircled by skeletal muscle, consistent with the external urethral sphincter (EUS). Skeletal muscle was absent at the level of the proximal urethra nearest the urethrovesical junction in one section. In the majority of sections examined, a midline gap in the external urethral sphincter muscle fibers was seen along the posterior

Table 1 Comparison of total, somatic, and autonomic nerve density in tissue sections at the level of the midurethra, proximal urethra, and upper trigone

	Anatomical region		Mid-urethra level (n=6)	Proximal urethra level (n=5)	Upper trigone level (n=3)	p value
Total nerve density	Vagina	Lateral	0.75 (0.49)	0.63 (0.31)	0.45 (0.09)	>0.99
		Medial	0.62 (0.48)	0.44 (0.23)	0.49 (0.16)	0.72
		Middle	0.74 (0.65)	0.55 (0.41)	0.53 (0.26)	0.72
	Periurethral/perivesical tissue	Lateral	0.58 (0.37)	0.50 (0.27)	0.76 (0.45)	0.10
		Medial	0.69 (0.56)	0.48 (0.17)	0.77 (0.31)	0.37
	Urethra	Skeletal muscle	0.60 (0.55)	0.65 (0.46)	–	0.65
		Smooth muscle	0.55 (0.55)	0.44 (0.43)	–	0.65
Somatic nerve density	Vagina	Lateral	0.04 (0.01)	0.043 (0.02)	0.03 (0.01)	0.61
		Medial	0.02 (0)	0.023 (0.01)	0.02 (0.01)	0.37
		Middle	0.04 (0.03)	0.05 (0.02)	0.02 (0.01)	0.10
	Periurethral/perivesical tissue	Lateral	0.09 (0.07)	0.08 (0.06)	0.14 (0.1)	0.10
		Medial	0.13 (0.14)	0.07 (0.03)	0.12 (0.13)	0.72
	Urethra	Skeletal muscle	0.15 (0.11)	0.19 (0.19)	–	0.18
		Smooth muscle	0.05 (0.03)	0.07 (0.05)	–	0.65
Autonomic nerve density	Vagina	Lateral	0.71 (0.48)	0.59 (0.31)	0.42 (0.1)	0.61
		Medial	0.60 (0.48)	0.41 (0.24)	0.47 (0.16)	0.72
		Middle	0.70 (0.63)	0.50 (0.41)	0.51 (0.26)	0.72
	Periurethral/perivesical tissue	Lateral	0.49 (0.34)	0.42 (0.23)	0.63 (0.35)	0.37
		Medial	0.56 (0.48)	0.41 (0.19)	0.64 (0.28)	0.37
	Urethra	Skeletal muscle	0.45 (0.48)	0.46 (0.5)	–	> 0.65
		Smooth muscle	0.50 (0.52)	0.38 (0.39)	–	0.65

Data are mean (%) ± SD

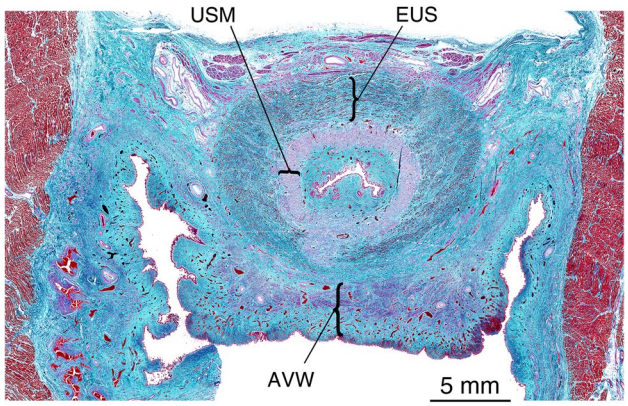

Fig. 2 Microscopic examination of urethral anatomy. Axial section at the level of the proximal urethra stained with Gomori Trichrome. The urethral smooth muscle (*USM*) is surrounded by the striated external urethral sphincter (*EUS*). Note a midline gap in the EUS on the dorsal aspect of the urethra and fusion of the anterior vaginal wall (*AVW*) with the urethral wall

(vaginal) side of the urethra (Fig. 2). This midline gap was absent in four sections (two from the midurethral and two from the proximal urethral levels) where skeletal muscle completely encircled the urethra. The lamina propria and vaginal muscularis layers of the anterior vaginal wall were identified in all sections examined. The adventitial layer was not consistently seen, and was particularly challenging to delineate in the "middle" sections of the vagina, where the urethral and vaginal wall appeared fused.

Total nerve density

The overall highest total (autonomic and somatic) nerve density was found at the level of the upper trigone, in the medial and lateral perivesical tissue, followed by the level of the midurethra, in the lateral and middle sections of the anterior vaginal wall (Table 1). When comparing anatomical sections within and between levels (midurethra, proximal urethra, and upper trigone) total nerve density was significantly different between sections of the vaginal wall at the midurethra level. It was highest in the lateral vagina, followed by the middle and medial vagina (mean 0.75%, SD ±0.49 vs 0.74%, SD ±0.65 vs 0.62%, SD ±0.48, p=0.03). Total nerve density did not significantly vary among the remaining sections analyzed (Table 1).

Autonomic nerve density

Overall, autonomic density was highest in the lateral and middle sections of the anterior vaginal wall at the midurethra level, followed by the perivesical tissue at the upper trigone level (Figs. 3, 4). Comparison of anatomical sections within and between levels demonstrated significant differences in the anterior vaginal wall at the midurethra level, where autonomic density was highest in the lateral section of the vagina, followed by the medial and middle sections respectively (0.71%, SD ±0.48 vs 0.70%, SD ±0.63 vs 0.60%, SD ±0.48, p= 0.03). Additionally, autonomic density was significantly higher in the lateral vaginal tissue than in the lateral periurethral tissue (0.59%, SD ±0.31 vs 0.42%, SD ±0.23, p=0.03) at the proximal urethra level. Autonomic nerve density did not vary significantly among the remaining sections analyzed (Table 1).

Somatic nerve density

Among all regions, somatic nerve density was highest in the skeletal muscle of the EUS (Fig. 5). When comparing anatomical sections, somatic density was significantly higher in the medial periurethral tissue than in the medial vagina (0.07%, SD ±0.03 vs 0.028%, SD ±0.01, p= 0.03) at the level of the proximal urethra. Somatic density was similar within the remaining sections analyzed (Table 1).

Comparison of autonomic and somatic density

Autonomic nerve density was higher than somatic nerve density in all regions examined at each anatomic level (Table 1). This difference was significant in all annotated sections at the mid- and proximal urethra level except for the skeletal muscle of the EUS. Autonomic and somatic density were not significantly different at the upper trigone level (results not shown).

Discussion

In this study of autonomic and somatic nerve density within the anterior vaginal wall and periurethral/perivesical tissue, autonomic and somatic nerve fibers were found in all annotated sections at all anatomical levels analyzed. The overall highest total and autonomic nerve density was in the perivesical tissue at the upper trigone level, and the lateral and middle regions of the anterior vaginal wall at the midurethra level. Overall somatic nerve density was highest in the skeletal muscle of the EUS.

Significant differences were noted in nerve density within the anterior vaginal wall where both total and autonomic density were highest in the lateral sections, followed respectively by the middle and medial sections. Total, autonomic and somatic nerve density were similar within the remaining sections analyzed at all anatomical levels, which likely reflects the diffuse branching of inferior hypogastric plexus and S2–S4 somatic nerve fibers within this tissue. Autonomic nerve density was significantly higher than somatic nerve density in all sections analyzed at the level of the mid- and proximal urethra, excluding the EUS.

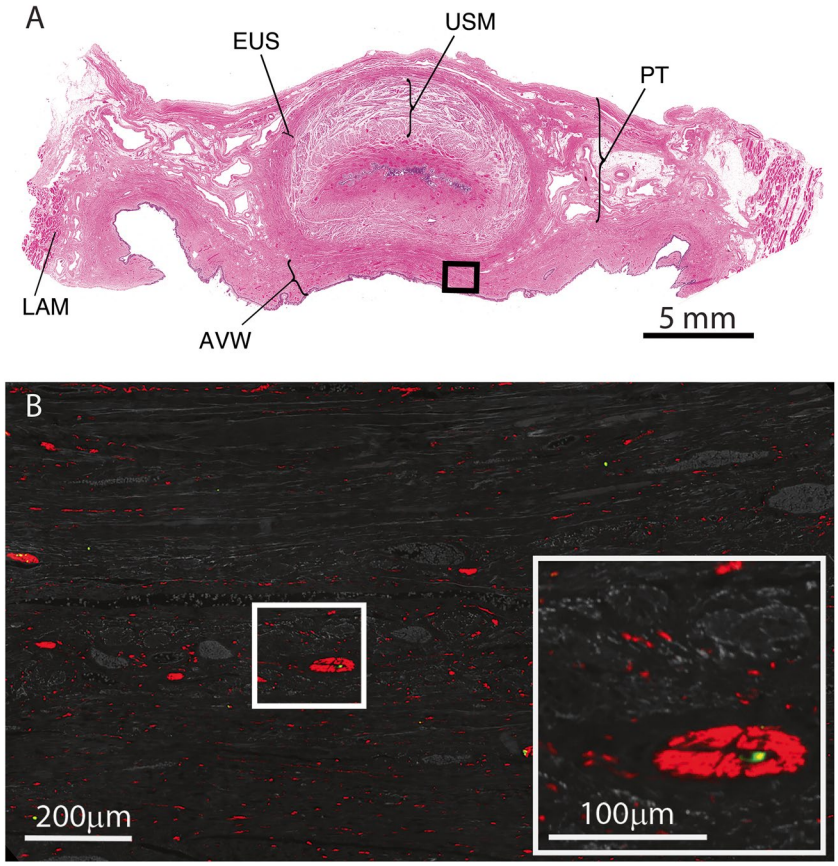

Fig. 3 Nerve density at midurethral level. Panel **A** shows hematoxylin and eosin (*H&E*) staining at the level of the midurethra. Key anatomical structures are labeled. *AVW* anterior vaginal wall, *EUS* external urethral sphincter, *LAM* levator ani muscle, *PT* periurethral tissue, *USM* urethral smooth muscle. Panel **B** shows the *boxed area* in panel **A** of the "middle" vaginal area from adjacent sections immunostained with antibodies against beta III tubulin (*βIIIT*), a general nerve marker, and myelin basic protein (*MBP*), a myelinated nerve marker. Unmyelinated autonomic nerve fibers are shown in *red* and myelinated somatic nerve fibers are shown in *green*, owing to the overlap of βIIIT and MBP staining. Tissue autofluorescence is shown in *gray* for structural reference. At this anatomical level, autonomic density was highest in the lateral and middle sections of the anterior vaginal wall. The *boxed area* within panel **B** represents an enlarged view of an autonomic nerve bundle

Several studies have published computer-generated three-dimensional models describing the location of autonomic and somatic nerves in fetal pelvic specimens [20–24]. According to these models, the uterovaginal nerve plexus, a component of the inferior hypogastric plexus, is primarily found on the anterolateral vaginal walls and posterolateral aspect of the urethra. Our findings of a relatively higher density of autonomic nerves within the perivesical tissue at the upper trigone level likely corresponds to extensions from the uterovaginal plexus. Additionally, relatively increased autonomic density in the lateral and middle sections of the anterior vaginal wall at the midurethral level likely represents the path of the cavernous nerves, the distal extensions of the inferior hypogastric plexus that ultimately supply the clitoris [24, 25]. The increased density of autonomic nerves in the middle vagina compared with the medial vagina may reflect crossover of the lateral fibers in the midline.

The EUS is supplied by somatic nerve fibers originating from S2–S4 that course along the inferior hypogastric plexus and pudendal nerve. Interestingly, autonomic and somatic nerve density in the skeletal muscle of the EUS was not significantly different, and in fact, autonomic density was higher. Karam and colleagues found that autonomic nerve fibers penetrate the skeletal muscle of the urethral sphincter in their path to reach the smooth muscle of the urethra [20]. This finding likely explains the relatively high density of autonomic nerve fibers within the skeletal muscle surrounding the urethra. Additionally, autonomic nerve fibers were noted on the periphery of vessel walls within the skeletal muscle.

Our findings of diffuse distribution of microscopic autonomic and somatic nerve fibers suggest that complete avoidance of nerve disruption during retropubic and anterior vaginal wall procedures might not be possible. In fact, two prior studies suggest that nerve disruption might occur along the path of trocars and mesh placed during midurethral sling procedures [13, 26]. Knowing this, minimizing the extent of tissue disruption may be the best strategy to reduce

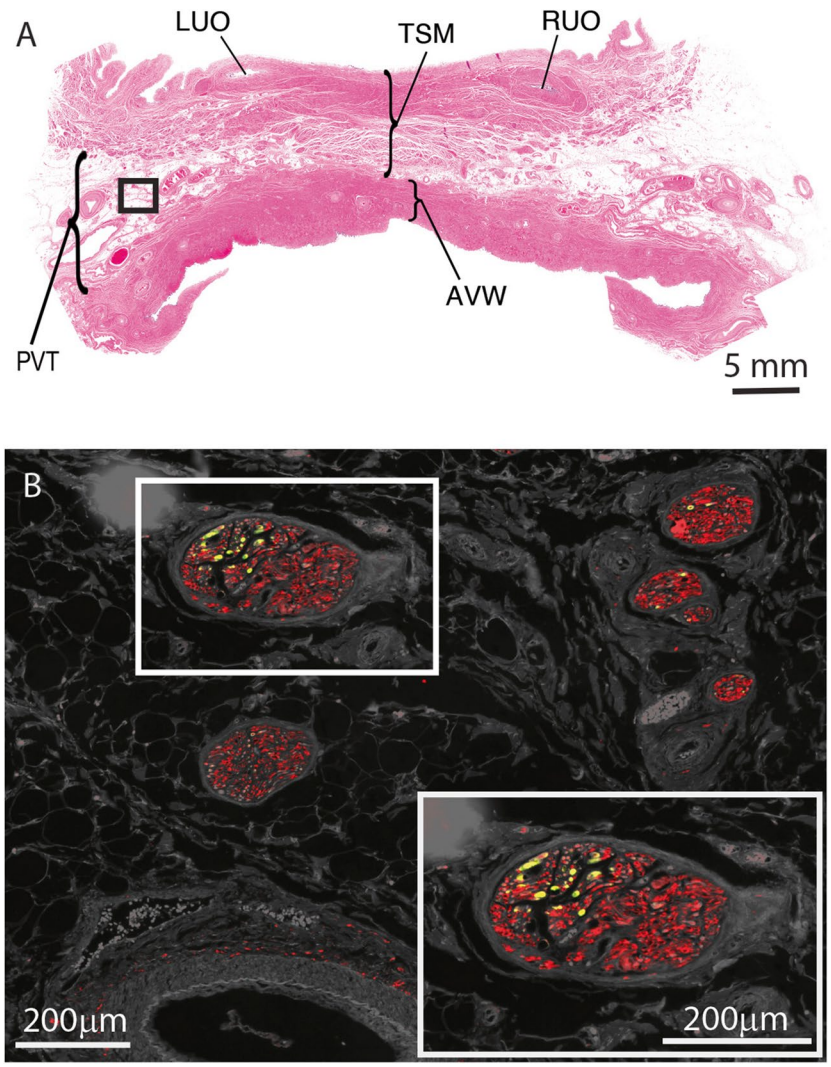

Fig. 4 Nerve density at the upper trigone level. Panel **A** shows hematoxylin and eosin (*H&E*) staining at the level of the upper trigone. Key anatomical structures are labeled. *AVW* anterior vaginal wall, *LUO* left ureteric orifice, *PVT* perivesical tissue, *RUO* right ureteric orifice, *TSM* trigone smooth muscle. Panel **B** shows the *boxed area* in panel **A** of PVT from adjacent sections immunostained with antibodies against beta III tubulin (*βIIIT*), a general nerve marker, and myelin basic protein (*MBP*), a myelinated nerve marker. Unmyelinated autonomic nerve fibers are shown in *red* and myelinated somatic nerve fibers are shown in *green*, owing to the overlap of βIIIT and MBP staining. Tissue autofluorescence is shown in *gray* for structural reference. At this anatomical level, autonomic density was highest in the periurethral tissue. The *boxed area* within panel **B** represents an enlarged view of autonomic nerve fibers mixed with somatic fibers

adverse postoperative outcomes such as voiding and sexual dysfunction.

During midurethral sling placement, vaginal dissection takes place along the middle section of the anterior vaginal wall, an area of relatively high autonomic nerve density, and the periurethral tissue. Strategies such as minimizing the width of tunnel creation and use of thin trocars may reduce disruption of nerve fibers in the anterior vaginal wall and periurethral tissue. Trocar passage should be performed within the lateral aspect of the periurethral tissue to avoid disrupting skeletal muscle fibers of the EUS along the lateral urethral wall as well as nerves coursing to supply the EUS within the medial periurethral tissue. Location of the lateral aspect of the periurethral tissue during retropubic procedures is facilitated by knowledge of the distance between the urethra and pelvic sidewall, and by direct palpation of the pelvic sidewall. In a cadaveric study, the average distance between the ATFP and the lateral aspect of the urethra 1 cm distal to the urethrovesical junction was 14 mm [19]. As the pelvis narrows distally, this distance is likely reduced at the level of the pubic symphysis; thus, trocar placement should typically not exceed a distance of 14 mm lateral to the urethra. Direct palpation of the pelvic sidewall aids in identification of the levator ani and can guide trocar placement just medial to the muscle. Perforation of levator ani muscle fibers was identified in 25% of retropubic sling procedures in a cadaveric study, which clinically may result in pelvic pain and sexual dysfunction [27]. Similarly, during colposuspension procedures, sutures should be placed in the lateral periurethral tissue and should not be tied down to avoid potential nerve compression. Entry to the retropubic space for pubovaginal slings requires larger perforation of the periurethral tissue at the level of the urethrovesical junction, which may lead to significant disruption of autonomic fibers coursing within the periurethral tissue. Strategies to minimize the degree of tissue disruption during this procedure also include use of thinner passing devices and perforation of the periurethral tissue as lateral to the urethra as possible.

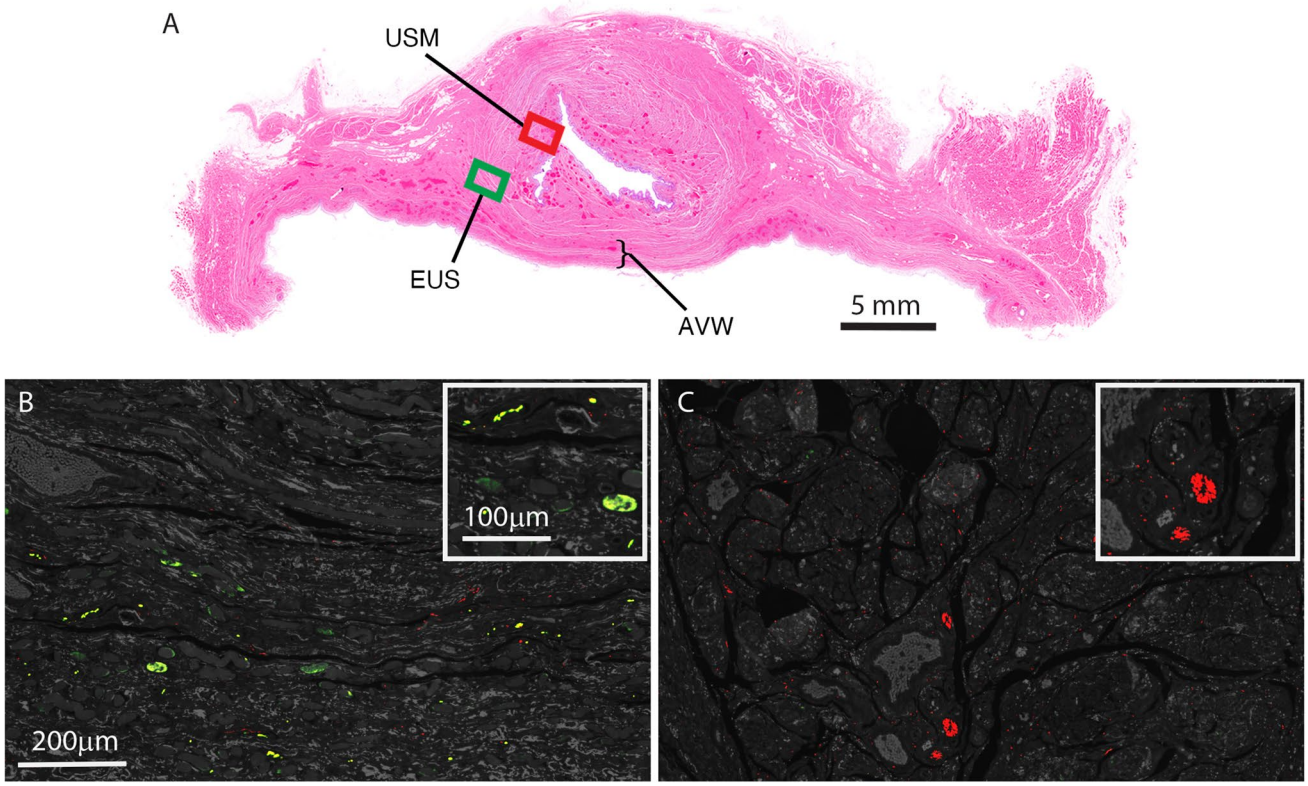

Fig. 5 Nerve density at the proximal urethral level. Panel **A** shows hematoxylin and eosin (*H&E*) staining at the level of the proximal urethra. Key anatomical structures are labeled. *AVW* anterior vaginal wall, *EUS* external urethral sphincter, *USM* urethral smooth muscle. Panel **B** shows the *green boxed area* in panel **A** of EUS and panel **C** shows the *red boxed area* in panel **A** of USM. Panels **B** and **C** represent adjacent sections immunostained with antibodies against beta III tubulin (*βIIIT*), a general nerve marker, and myelin basic protein (*MBP*), a myelinated nerve marker. Unmyelinated autonomic nerve fibers are shown in *red* and myelinated somatic nerve fibers are shown in *green*, owing to the overlap of βIIIT and MBP staining. Tissue autofluorescence is shown in gray for structural reference. At this anatomical level, somatic nerve density was highest in the skeletal muscle of the EUS. The *boxed area* within panel **B** represents an enlarged view of somatic nerves within the EUS. The *boxed area* within panel **C** represents an enlarged view of autonomic fibers within the USM

Strengths of this study included a comprehensive evaluation of young, nulliparous cadavers that are often difficult to obtain. These characteristics help to provide a baseline for analysis of changes possibly caused by parity and menopause. Tissue harvesting was performed within 24 h of death, which reduces tissue damage potentially associated with repetitive tissue freezing and cellular lysis. Most prior immunostaining studies of the vagina and periurethral tissue have been performed in fetal specimens and have provided information regarding the general location of nerve subtypes within these areas of interest, but have not quantified the relative density of nerve subtypes [21–24]. Among the limited studies reporting quantitative data, overall nerve density is most commonly determined by manual nerve counts from small tissue areas that are extrapolated to describe the nerve density of larger regions [17, 28]. Thus, our use of whole mount slide, multichannel images arguably provides the most sensitive and comprehensive form of analysis of nerve density in this region. However, this experimental method of nerve density analysis in such large sections of adult pelvic tissue requires future studies to confirm and expand upon our overall findings.

Limitations include those inherent to cadaver studies, including limited demographic data and alterations in tissue quality and composition compared with in vivo tissue. The majority of cadavers examined were white nulliparous females, which may limit the generalizability of our results to underrepresented minority groups and multiparous patients. A small sample size and wide variation in nerve density among cadavers potentially reduce the strength of our analysis.

Conclusion

Autonomic and somatic nerves are located diffusely within the urethra, periurethral tissue and anterior vaginal wall, with increased density of autonomic fibers in the middle

and lateral aspects of the vaginal wall, and somatic fibers in the skeletal muscle of the EUS. Such distribution likely reflects the diffuse branching of inferior hypogastric nerve fibers and somatic efferents from S2–S4 that comprise the primary source of autonomic and somatic nerve supply respectively in this region. Although complete avoidance of nerve disruption during retropubic and anterior vaginal wall procedures is likely inevitable, minimizing tissue disruption close to the urethral skeletal muscle and autonomic nerve fibers within the anterior vaginal wall may avert compromise of urinary continence and possibly sexual response mechanisms. Future studies including greater representation of older and parous cadavers may provide further insight into the respective impact of age and trauma associated with childbirth on the neuroanatomy of the anterior vaginal wall and periurethral tissue.

Acknowledgements We thank the UT Southwestern Medical Center Willed Body Program, Jessica Williams of the UT Southwestern Histo Pathology Core for super-large-format histological processing, sectioning, and staining. We thank Li Li and Ariana Nawaby for contributions to immunostaining, and the UT Southwestern Whole Brain Microscopy Facility (WBMF; RRID: SCR_017949) for assistance with whole-slide imaging and analyses.

Authors' contributions E.E. Tappy: project development, data collection and analysis, manuscript writing; D.M.O. Ramirez: project development, data collection and analysis, manuscript writing; A.M. Stork: data collection, manuscript writing; K.S. Carrick: project development, data collection and analysis, manuscript writing; J.J. Hamner: data collection, manuscript writing; J. Pruszynski: data analysis, manuscript writing; M.M. Corton: project development, data collection and analysis, manuscript writing.

Declarations

Conflicts of interest None.

References

1. Schimpf MO, Rahn DD, Wheeler TL, Patel M, White AB, Orejuela FJ, et al. Sling surgery for stress urinary incontinence in women: a systematic review and metaanalysis. Am J Obstet Gynecol. 2014;211(1):71 e1–e27.
2. Ford AA, Taylor V, Ogah J, Veit-Rubin N, Khullar V, Digesu GA. Midurethral slings for treatment of stress urinary incontinence review. Neurourol Urodyn. 2019;38(Suppl 4):S70–S5.
3. Szell N, Komisaruk B, Goldstein SW, Qu XH, Shaw M, Goldstein I. A meta-analysis detailing overall sexual function and orgasmic function in women undergoing midurethral sling surgery for stress incontinence. Sex Med. 2017;5(2):e84–93.
4. Cayan F, Dilek S, Akbay E, Cayan S. Sexual function after surgery for stress urinary incontinence: vaginal sling versus Burch colposuspension. Arch Gynecol Obstet. 2008;277(1):31–6.
5. Christmann-Schmid C, Koerting I, Ruess E, Faehnle I, Krebs J. Functional outcome after laparoscopic nerve-sparing sacrocolpopexy: a prospective cohort study. Acta Obstet Gynecol Scand. 2018;97(6):744–50.
6. Turner LC, Kantartzis K, Shepherd JP. Predictors of postoperative acute urinary retention in women undergoing minimally invasive sacral colpopexy. Female Pelvic Med Reconstr Surg. 2015;21(1):39–42.
7. Antosh DD, Megahed NN. Sexual Function After Pelvic Reconstructive Surgery. ObstetGynecol Clin North Am. 2021;48(3):639–51.
8. Zyczynski HM, Rickey L, Dyer KY, Wilson T, Stoddard AM, Gormley EA, et al. Sexual activity and function in women more than 2 years after midurethral sling placement. Am J Obstet Gynecol. 2012;207(5):421 e1–6.
9. Glass Clark SM, Huang Q, Sima AP, Siff LN. Effect of Surgery for Stress Incontinence on Female Sexual Function. Obstet Gynecol. 2020;135(2):352–60.
10. Ripperda CM, Jackson LA, Phelan JN, Carrick KS, Corton MM. Anatomic relationships of the pelvic autonomic nervous system in female cadavers: clinical applications to pelvic surgery. Am J Obstet Gynecol. 2017;216(4):388 e1–e7.
11. Aurore V, Rothlisberger R, Boemke N, Hlushchuk R, Bangerter H, Bergmann M, et al. Anatomy of the female pelvic nerves: a macroscopic study of the hypogastric plexus and their relations and variations. J Anat. 2020;237(3):487–94.
12. Montoya TI, Calver L, Carrick KS, Prats J, Corton MM. Anatomic relationships of the pudendal nerve branches. Am J Obstet Gynecol. 2011;205(5):504 e1–5.
13. Bekker MD, Hogewoning CR, Wallner C, Elzevier HW, DeRuiter MC. The somatic and autonomic innervation of the clitoris; preliminary evidence of sexual dysfunction after minimally invasive slings. J Sex Med. 2012;9(6):1566–78.
14. Barber MD, Visco AG, Wyman JF, Fantl JA, Bump RC, Continence Program for Women Research G. Sexual function in women with urinary incontinence and pelvic organ prolapse. Obstet Gynecol. 2002;99(2):281–9.
15. Mistry MA, Klarskov N, DeLancey JO, Lose G. A structured review on the female urethral anatomy and innervation with an emphasis on the role of the urethral longitudinal smooth muscle. Int Urogynecol J. 2020;31(1):63–71.
16. Hilliges M, Falconer C, Ekman-Ordeberg G, Johansson O. Innervation of the human vaginal mucosa as revealed by PGP 9.5 immunohistochemistry. Acta Anat (Basel). 1995;153(2):119–26.
17. Li T, Liao Q, Zhang H, Gao X, Li X, Zhang M. Anatomic distribution of nerves and microvascular density in the human anterior vaginal wall: prospective study. PLoS One. 2014;9(11):e110239.
18. Mazloomdoost D, Westermann LB, Mutema G, Crisp CC, Kleeman SD, Pauls RN. Histologic anatomy of the anterior vagina and urethra. Female Pelvic Med Reconstr Surg. 2017;23(5):329–35.
19. Hamner JJ, Carrick KS, Ramirez DMO, Corton MM. Gross and histologic relationships of the retropubic urethra to lateral pelvic sidewall and anterior vaginal wall in female cadavers: clinical applications to retropubic surgery. Am J Obstet Gynecol. 2018;219(6):597 e1–e8.
20. Karam I, Droupy S, Abd-Alsamad I, Uhl JF, Benoit G, Delmas V. Innervation of the female human urethral sphincter: 3D reconstruction of immunohistochemical studies in the fetus. Eur Urol. 2005;47(5):627–33; discussion 34.
21. Yucel S, De Souza A, Jr., Baskin LS. Neuroanatomy of the human female lower urogenital tract. J Urol. 2004;172(1):191–5.
22. Alsaid B, Moszkowicz D, Peschaud F, Bessede T, Zaitouna M, Karam I, et al. Autonomic-somatic communications in the human pelvis: computer-assisted anatomic dissection in male and female fetuses. J Anat. 2011;219(5):565–73.
23. Moszkowicz D, Alsaid B, Bessede T, Penna C, Benoit G, Peschaud F. Female pelvic autonomic neuroanatomy based on conventional macroscopic and computer-assisted anatomic dissections. Surg Radiol Anat. 2011;33(5):397–404.
24. Moszkowicz D, Alsaid B, Bessede T, Zaitouna M, Penna C, Benoit G, et al. Neural supply to the clitoris: immunohistochemical study with three-dimensional reconstruction of cavernous

nerve, spongious nerve, and dorsal clitoris nerve in human fetus. J Sex Med. 2011;8(4):1112–22.
25. Marino VDLH. Anatomic study of the clitoris and the bulbo-clitoral organ. Basel, Switzerland: Springer International Publishing; 2014.
26. Giovannetti O, Tomalty D, Gaudet D, Clohosey D, Forster A, Monaghan M, et al. Immunohistochemical investigation of autonomic and sensory innervation of anterior vaginal wall female periurethral tissue: a study of the surgical field of mid-urethral sling surgery using cadaveric simulation. J Sex Med. 2021;18(7):1167–80.
27. Rahn DD, Marinis SI, Schaffer JI, Corton MM. Anatomical path of the tension-free vaginal tape: reassessing current teachings. Am J Obstet Gynecol. 2006;195(6):1809–13.
28. Aydin S, Sonmez FC, Karasu AFG, Gul B, Arioglu C. Search for the G spot: microvessel and nerve mapping of the paraurethral anterior vaginal wall. Int Urogynecol J. 2020;31(12):2565–72.